MIT Libraries | DSpace@MIT

MIT Open Access Articles

Electrolyte Competition Controls Surface Binding of CO Intermediates to CO 2 Reduction Catalysts

The MIT Faculty has made this article openly available. ***Please share*** how this access benefits you. Your story matters.

Citation: Wuttig, Anna, Ryu, Jaeyune and Surendranath, Yogesh. 2021. "Electrolyte Competition Controls Surface Binding of CO Intermediates to CO 2 Reduction Catalysts." Journal of Physical Chemistry C, 125 (31).

As Published: 10.1021/ACS.JPCC.1C04337

Publisher: American Chemical Society (ACS)

Persistent URL: https://hdl.handle.net/1721.1/141325

Version: Original manuscript: author's manuscript prior to formal peer review

Terms of use: Creative Commons Attribution-Noncommercial-Share Alike

Massachusetts Institute of Technology

Electrolyte Competition Controls Surface Binding of CO Intermediates to CO_2 Reduction Catalysts

Anna Wuttig,[1,†] Jaeyune Ryu,[1] and Yogesh Surendranath[1]*

[1]Department of Chemistry, Massachusetts Institute of Technology, Cambridge, Massachusetts, United States

ABSTRACT: Adsorbed CO is a critical intermediate in the electrocatalytic reduction of CO_2 to fuels. Directed design of CO_2RR electrocatalysts have centered on strategies to understand and optimize the differences in CO adsorption enthalpy across surfaces. Yet, this approach has largely ignored the role of competitive electrolyte adsorption in defining the CO surface population relevant for catalysis. Using *in situ* infrared spectroelectrochemistry, we disclose the contrasting influence of electrolyte competition on reversible CO binding to Au and Cu catalysts. Whereas reversible CO binding to Au surfaces is driven by substitution and reorientation of adsorbed water, CO binding to Cu surfaces requires the reductive displacement of adsorbed carbonate anions. The divergent role of electrolyte competition for CO adsorption on Au vs. Cu leads to a ~600 mV difference in the potential region where CO accumulates on the two surfaces. The contrasting CO adsorption stoichiometry on Au and Cu also explains their disparate reactivity: water adsorption drives CO liberation from Au surfaces, impeding further reduction, whereas carbonate desorption drives CO accumulation on Cu surfaces, allowing for further reduction to hydrocarbons. These studies provide direct insight into how electrolyte constituents can serve as powerful design parameters for fine-tuning of CO surface populations and, thereby, CO_2-to-fuels reactivity.

INTRODUCTION

CO_2 electroreduction would allow for the storage of intermittent renewable electricity in energy-dense chemical fuels.[1,2] The dominant mechanistic paradigm for CO_2 reduction at heterogeneous catalysts invokes surface bound CO as a critical intermediate. Thus, the surface population of and the catalyst's affinity for CO are expected to correlate with the efficiency and selectivity of fuel formation. Indeed, it has been postulated that a catalyst's CO affinity determines whether this key intermediate is liberated as the final product or reduced further to higher order hydrocarbons and oxygenates.[3–5] Furthermore, theoretical studies establish that CO affinities also scale linearly with the adsorption energies of other CO_2RR intermediates,[4,6,15–18,7–14] suggesting that the CO adsorption energy is a powerful descriptor of CO_2RR reactivity.[19] Despite the widespread appreciation of the importance of CO adsorption thermodynamics, it has not been directly examined and compared for various CO_2 reduction catalysts under electrochemical conditions. Instead, the CO adsorption energy of various known and postulated catalysts have been inferred primarily from theoretical studies[4,7,14,20] or ultra-high vacuum (UHV) analysis.[17] However, both of these methods apply a simple gas-solid model of adsorption, in which CO binds to unoccupied surface sites (**Scheme 1a**).[7]

This gas-solid model does not accurately represent the CO binding chemistry that dominates during catalysis at a polarized solid-liquid interface. Under reaction conditions, CO binding, by necessity, involves the displacement and/or rearrangement of solvent (**Scheme 1b**, *S*) and electrolyte ions (**Scheme 1 b**, A^{n-}), and this aggregate equilibrium defines the CO surface population.[21] Critically, analysis of the potential-dependence of CO binding must consider the key roles of *S* and/or A^{n-} because changes in the magnitude and sign of the interfacial electric field alters the stability of solvent dipoles and/or drives electron-transfer-mediated ion adsorption or desorption.[22–25] It is well-established that the potential-dependent binding of *S* and/or A^{n-} alters the surface's affinity for neutral small molecules such as benzene and ethylene.[21–29] This precedent suggests that the potential-dependent affinity of the surface for competing water and electrolyte ions (e.g. (bi)carbonate) is expected to be dominant contributors in defining the CO surface population during CO_2RR. Yet, a systematic understanding of how competing adsorption reactions contribute to the potential-dependence of CO binding (**Scheme 1b**) across materials remains elusive. Together, these knowledge gaps impede directed efforts to control CO affinity and tune CO_2RR selectivity.

Here, we probe the CO adsorption stoichiometry by simultaneously tracking the adsorption of CO, water, and (bi)carbonate using *in-situ* surface-enhanced infrared absorption spectroscopy (SEIRAS) in an attenuated total reflectance (ATR) mode.[30–33] In SEIRAS, nanostructured electrode surfaces amplify IR absorption by adsorbed molecules with transition dipole moments perpendicular to the surface.[30–33] This technique is ideally suited to quantify CO affinity *in situ* because ATR-SEIRAS provides: (a) linear response in adsorbate coverage and

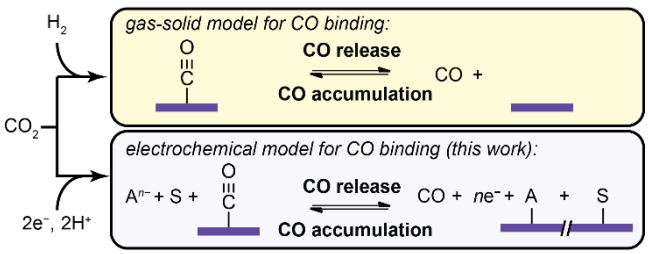

Scheme 1. (**a**) Gas-solid model for CO binding in ultra-high vacuum. (**b**) Electrochemical model for CO binding shown here.

signal intensity;[34] (b) large spectral range; and (c) unrestricted mass transport to the catalyst surface.

We use SEIRAS to compare the reversible CO adsorption stoichiometry on Au and Cu CO_2RR catalysts. Au and Cu offer an ideal platform for investigating these differences because (1) they display reversible CO binding under electrochemical conditions[35–40] and (2) they display radically different CO_2RR product distributions. Au catalyses the production of CO as the major product[41] whereas Cu is unique in catalysing the formation of CH_4 and C_2H_4[42]. This divergent reactivity has been explained by a difference in the enthalpy of CO adsorption computed on idealized closed-packed Au and Cu surfaces in UHV (~30 kJ mol^{-1}),[4] where the weak Au-CO bond favors liberation of CO as the major product and the stronger adsorption to Cu allows for accumulation of this intermediate. However, these UHV-derived enthalpy values are insufficient to explain the potential-dependence of CO adsorption on the two surfaces[35–40] and there exist varying perspectives on the role of the electrolyte in gating CO binding on these materials.[37,38,43] Thus, we were motivated to identify and determine the potential-dependence of competing solvent and electrolyte ion interactions that define the CO population on these two surfaces under common CO_2RR conditions. We show that the divergent reactivity profiles of Au and Cu can be explained by differing solvent/electrolyte reaction equilibria. On Au surfaces, water adsorption drives CO liberation, impeding further reduction. In contrast, on Cu surfaces, carbonate desorption drives CO accumulation, allowing for further reduction to hydrocarbons. These studies provide a molecular basis for explaining how competing surface reactions contribute to differential potential-dependent CO surface populations across materials.

RESULTS AND DISCUSSION

CO Binding Equilibria on Polarized Au Surfaces. We investigated the CO adsorption dynamics on Au films in CO-saturated 0.1 M (bi)carbonate buffer, pH 9.2, (unless otherwise stated, all data collected employ this electrolyte, C_i). At this alkaline pH, the low equilibrium concentration of CO_2 minimizes convoluting CO_2RR,[38] and consistent with negligible CO_2RR, we observe featureless SEIRA spectra in the CO region, 1700 to 2200 cm^{-1} when using Ar-saturated C_i (**Figure S1**). **Figures 1a** and **b** show the cyclic voltammogram (CV) and SEIRA spectra of a Au film, where the background was recorded at –1.00 V under CO-saturation (this potential was chosen for reasons discussed in the SI and **Figure S2**). We observe a peak at 2079 cm^{-1} that appears at –0.57 V, reaches a maximum value at –0.14 V (**Figure 1c**), and declines monotonically at more positive potentials. This peak exhibits a 49 cm^{-1} V^{-1} Stark tuning slope, **Figure S3a**. Both the Stark tuning slope and the band position are in line with our previous assignment of linearly-bonded CO to Au (CO_{atop}).[36] On the reverse-going (blue) trace, the potential-dependence of the CO_{atop} band is identical to the forward-going (red) trace, **Figure 1c**, indicating that CO_{atop} exhibits reversibility with respect to changes in applied potential. In addition, we observe that the CO_{atop} population increases as the potential is swept from –1.00 to –0.14 V and then decays in a symmetric fashion as the applied potential approaches 0.04 V (**Figure 1c**). We find that as the P_{CO} is reduced, the population of CO_{atop} at a given potential systematically decreases, indicative of reversible CO_{atop} binding under these conditions (**Figure 2a** and **S4**). Other observed CO binding motifs are irreversible and described in **Figures S2-6**, and the SI. We note that the relative band intensities of CO_{atop} to the irreversible bands differ from that observed previously by our group[44] and others[38,45]. In our study, we employ Au counter electrodes and purified ultra-high-purity electrolytes (see SI for detailed experimental procedures). We also performed a control experiment with a Pt counter electrode and observe no spectra differences (**Figure S6**), further ruling out the possibility of contaminants from the counter electrode[38,45] in our experimental setup. Nonetheless, we acknowledge that our spectra do vary from those reported by others and we postulate that these variations could result from differences in Au SEIRAS film preparation (see synthesis procedure in the SI) that appear to lead to an enrichment in Au(110) facets (**Figure S7**), known to display CO_{hollow}, CO_{bridge}, and CO_{atop} in intensity ratios comparable[46] to what we observe. Additionally, the following analysis of CO binding stoichiometry is restricted to the reversible CO_{atop} band, which displays potential dependent adsorption over the same range of potentials observed by others[38,45] irrespective of the presence or absence of irreversible CO bands." Thus, the foregoing analyses focus on the reversible CO_{atop} band.

The potential dependence of reversible CO_{atop} electrosorption at every P_{CO} examined exhibits a bell-shape behavior. This behavior is a well-documented phenomenon for the electrosorption of various organic molecules in aqueous electrolytes.[26,28,29] Theoretical models capture this bell-shape dependence by describing the electrosorption process as a competition between the adsorption and reorientation of interfacial water and the adsorption of the organic molecule.[21–27] Due to the relatively large dipole moment of water (1.83 D), the models predict that the potential-dependence of organic molecules reflects changes in

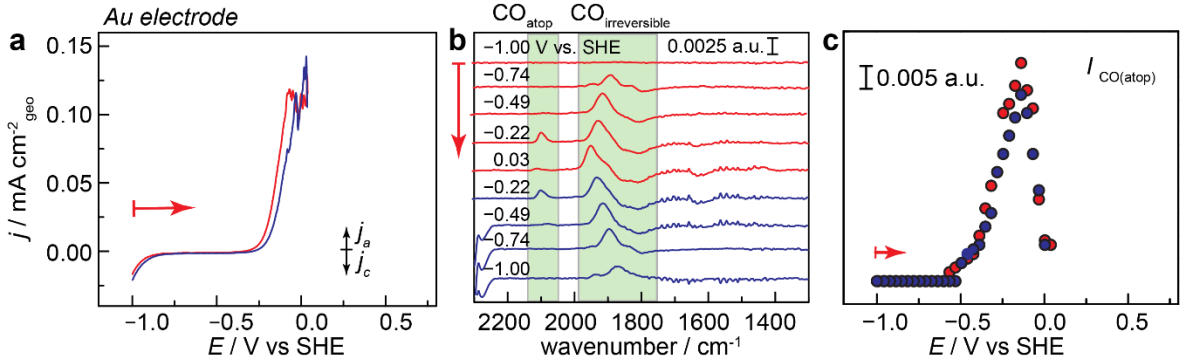

Figure 1. (**a**) Cyclic voltammogram (CV) obtained on a Au film at 2 mVs^{-1} in 1.00 atm CO-saturated 0.1 M sodium bicarbonate electrolyte, pH 9.2 ± 0.1, 24 ± 1 ℃ (**a**). CV scans were initiated at –1.00 V vs. SHE in a positive-going (**red**) direction and the reverse negative-going (**blue**) direction is also shown. (**b**) Simultaneously acquired SEIRA spectra with the shaded regions denoting peaks corresponding to reversible, CO_{atop}, and irreversible CO adsorption. (**c**) Integrated band intensities for adsorbed CO_{atop}. Background spectra were recorded at –1.00 V.

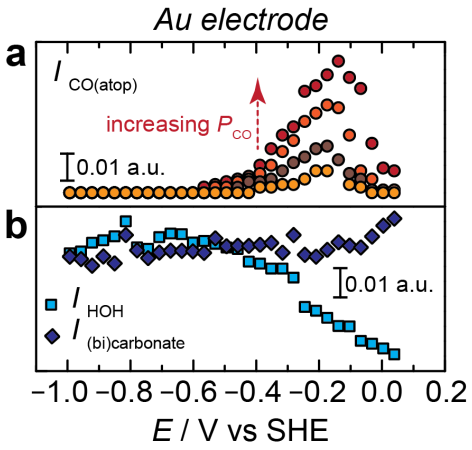

Figure 2. (**a**) Integrated CO_{atop} band intensities on a Au electrode as a function of CO partial pressure at 0.13 (yellow circles), 0.25 (brown circles), 0.50 (orange circles), and 1.00 atm (red circles) CO with Ar as the balance gas. (**b**) Integrated band intensity for the H-O-H bending mode of interfacial water (dark blue squares) and adsorbed carbonate (light blue diamonds). Data recorded in 1.00 atm CO-saturated 0.1 M sodium bicarbonate buffer electrolyte, pH 9.2 ± 0.1, 24 ± 1 ℃, where CV scans were initiated at –1.0 V vs. SHE. The forward-going trace is reported.

the aggregate orientation of interfacial water dipole moments as the applied potential is swept positive and negative of the potential of zero-charge (PZC).[21–27] Thus, maximum adsorption is expected at the PZC of the working electrode, where the interfacial field is the weakest. Our observation of a bell-shaped potential dependence of CO_{atop} electrosorption suggests that this model could also describes the system examined here. Indeed, the peak potential (E_{max}) of the bell-shaped curve at –0.14 V corresponds to the measured PZC of Au of around –0.10 V[47] in $NaClO_4$ electrolytes. We note that the decrease in the CO_{atop} population observed at potential values more positive that 0.00 V could reflect CO depletion near the electroactive surface due to Au-catalyzed CO oxidation (**Figure 1a**). We exclude this possibility because, upon overlaying the CO oxidation CV trace with the CO_{atop} band intensity (**Figure S8**), we see that CO oxidation current continues to rise even as the CO_{atop} band intensity falls rapidly. Indeed, the rising CO oxidation current does not become transport-limited until 0.00 V and at which point the CO_{atop} band has already declined for ~140 mV. In addition, we note that possibility that cation adsorption may be contributing to a decline in the CO_{atop} band. It has been observed that hydrophobic cations, such as tetramethylammonium[38], display increased spectroscopic band intensity at potentials lower than –0.25 V vs SHE on Au. This potential for cation adsorption is 90 mV more negative than the peak potential for CO_{atop} adsorption, –0.14 V, and we would expected the cation adsorption potential to be shifted even more negative for the more hydrophilic Na^+ used in this study. Thus, we postulate that the dominant factor leading to the decline in CO_{atop} band is interfacial water reorientation. Together, this analysis suggests that interfacial water reorientation mediates CO binding.

Additional insight in this process is obtained from direct analysis of the interfacial water band. At –0.22 V, we observe a bleach at 1616 cm^{-1} (**Figure 1b**). Based on previous SEIRAS studies,[48–50] we assign this band to δHOH bending mode of interfacial water canted towards the surface as depicted in **Figure 3a**, left. **Figure 2b** shows that the integrated band intensity corresponding to this δHOH bending mode of interfacial water (light blue squares) remains roughly constant from –1.00 V to –0.57 V and then decreases roughly linearly as the electrode potential approaches 0.04 V. The decrease in integrated band intensity indicates that this canted interfacial water is either (1) re-orientating to an IR-inactive position (**Figure 3a**, middle), and/or (2) dissociating from the surface. This behavior describes the molecular structure of water up until the PZC. At potentials more positive than the PZC, the rebinding of the water would be expected to accompany CO dissociation. However, this adsorption does not lead to an increase in the interfacial water band intensity because water would rebind in a different, canted-up orientation (**Figure 3a**, right), giving rise to a red-shifted δHOH bending mode relative to the canted-down orientation.[48] Since the background is collected at potentials negative of the PZC, this red-shifted rebinding results in a continued decline in the intensity of the δHOH bending mode at potential values more positive than PZC (**Figure 2b**, light blue squares). Thus, the strong correlation of the water band with CO_{atop} binding further evinces that potential-dependent changes in the orientation and population of interfacial water drive CO adsorption.

CO_{atop} adsorption on Au is not correlated with changes in the surface population of (bi)carbonate. At 0.03 V, we observe a peak at 1442 cm^{-1}, which is attributed to the A_1 mode of adsorbed monodentate carbonate[51–54]. Unlike water, the band intensity corresponding to the adsorbed carbonate remains roughly constant across the entire potential range, and only begins to appreciably increase at 0.00 V, a potential value 160 mV past the peak of maximum CO_{atop} adsorption, **Figure 2b**, dark blue diamonds. Indeed, if carbonate adsorption were gating the desorption of CO_{atop}, we would expect to see a dramatic rise in the IR signatures for carbonate that matched the decline in CO_{atop} band, as observed for Cu, see below. Thus, while we cannot unequivocally rule out the role of carbonate adsorption at the tail end of the CO_{atop} desorption profile, we postulate that water

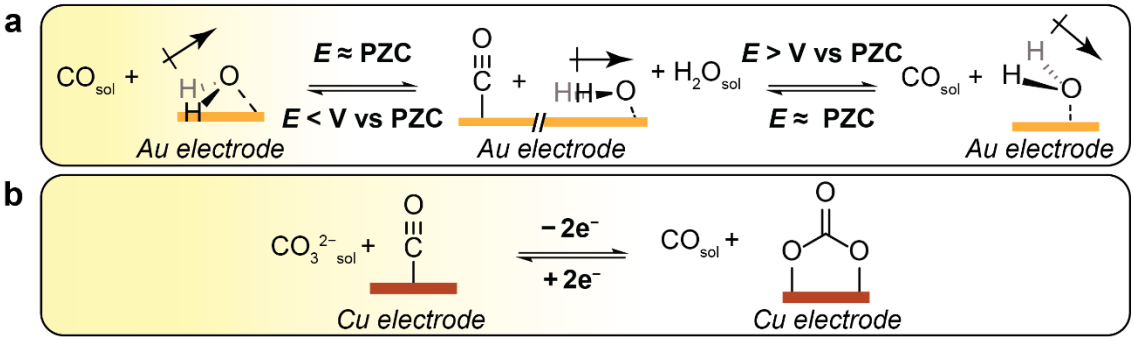

Figure 3. (**a**) Proposed stoichiometry of potential-dependent CO binding on Au relative to the potential of zero charge (PZC). (**b**) Proposed stoichiometry of CO binding to Cu surfaces. The yellow region to the left of each panel denotes the dominant speciation in the reductive potential-region relevant to CO_2RR catalysis.

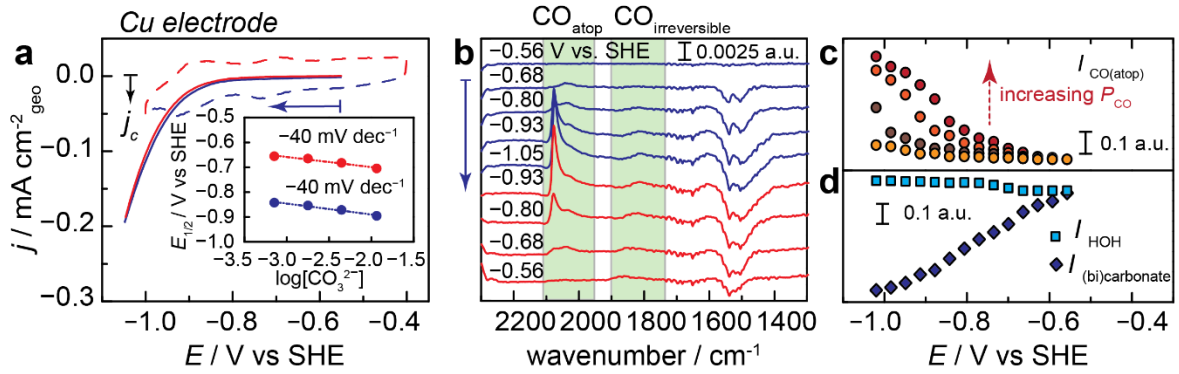

Figure 4. (**a**) Cyclic voltammograms (CV) obtained on a Cu film at 2 mV s^{-1} in 1.00 atm CO-saturated 0.1 M sodium bicarbonate electrolyte, pH 9.2 ± 0.1, 24 ± 1 ℃. CV scans were initiated at –0.56 V vs SHE in a negative-going (solid line, blue) direction. Overlaid CV obtained on a Cu foil recorded at 350 mV s^{-1} and initiated at –0.43 V in a negative-going (dotted line, blue) direction. Half-wave potential ($E_{1/2}$) of the two voltammetric waves vs logarithm of the carbonate concentration (inset). (**b**) Simultaneously acquired SEIRA spectra for the Cu film with the shaded regions denoting peaks corresponding to reversible, CO_{atop}, and irreversible CO adsorption. (**c**) Integrated CO_{atop} band intensities as a function of CO partial pressure at 0.13 (yellow circles), 0.25 (brown circles), 0.50 (orange circles), and 1.00 (red circles) atm CO with Ar as the balance gas. (**d**) Integrated band intensity for the H-O-H bending mode of interfacial water (light blue squares) and adsorbed (bi)carbonate (dark blue diamonds).

adsorption and reorientation are the primary contributors to the binding and release of CO_{atop} on Au. In addition, we do not observe voltammetric features associated with compensatory charge flow upon desorption of (bi)carbonate (see below for a corresponding discussion on Cu). Together, these results suggest that the potential-dependence of CO_{atop} electrosorption to Au is correlated with changes in the orientation and population of interfacial water and not carbonate.

The forgoing analysis is consistent with the model for CO_{atop} binding on Au surfaces schematically shown in **Figure 3a**. At potentials negative of the PZC, interfacial water populates the Au surface in a canted-down orientation. At the PZC, the weak interfacial field no longer stabilized water dipoles, thus CO_{atop} binding becomes favourable. At potentials positive of the PZC, water dipoles can be stabilized in a canted-up orientation, driving off CO from the surface. This reaction stoichiometry highlights that the energetics of water adsorption and reorientation drives the potential-dependence of CO_{atop} electrosorption on Au surfaces.

CO Binding Equilibria on Polarized Cu Surfaces. With a description of the molecularity of CO adsorption on Au in hand, we performed similar experiments on Cu surfaces to provide insight into the molecularity of CO electrosorption on a different CO_2RR electrocatalysts with radically different product selectivity. The slightly alkaline C_i conditions employed to study CO electrosorption on Au surfaces also lead to negligible convolution from CO_2RR on Cu surfaces, **Figure S9**, and therefore all observed CO peaks are interpreted as resulting from intentionally added CO. **Figure 4a** and **b** shows the CV and simultaneously collected SEIRA spectra, respectively, in CO-saturated C_i electrolyte. The background spectrum was collected at –0.56 V. Beginning at –0.68 V, we observed the appearance of a peak at 2043 cm^{-1}. This feature exhibits a Stark tuning slope of 26 cm^{-1} V^{-1} (**Figure S10a**) and increases in intensity as the potential is swept more negative. Beginning at –0.80 V, we observed the rise of a shoulder peak at 2075 cm^{-1} that displays a negligible Stark tuning slope. The aggregate intensity of both bands continue to rise monotonically with increasingly negative potentials within the full range of conditions tested (–0.56 V to –1.05 V) (**Figure 4c**). At high P_{CO} values greater than 0.5 atm, the aggregate intensity of both bands reaches a maximum value at –1.01 V (**Figure 4c**). The frequency range of this aggregate CO band is in line with the 1990 to 2100 cm^{-1} range reported for linearly bonded CO on Cu in UHV, and thus we denote the cumulative CO band as CO_{atop}.[55–57] On the reverse-going CV sweep, the CO_{atop} band declines in intensity with a profile very similar to that observed for its rise on the negative-going trace (**Figure S11**). These findings indicate that CO_{atop} binding is reversible with respect to changes in applied potential. In addition, we observe that the magnitude of the CO_{atop} band monotonically increases with increasing P_{CO} at fixed potential values (**Figures 4c** and **S12**). The P_{CO} dependence of this band provides further evidence for the reversibility of CO_{atop} electrosorption to Cu under these conditions. The spectra also contain peaks corresponding to other binding motifs of CO,[58] but all of these are irreversible with respect to changes in potential (see **Figures S10**, **S11**, and the SI). In order to the extract thermochemical information about reversible CO adsorption on Cu, we, therefore, restrict the foregoing analysis to the CO_{atop} band.

CO_{atop} electrosorption correlates with carbonate desorption. At potentials more negative than –0.68 V, we observe a bleach at 1543 and 1509 cm^{-1} (**Figure 4b**). These bands are assigned to the A_1 and B_2 modes, respectively, of carbonate adsorbed to Cu in a bidentate mode bridging two copper centers.[51–54,59] The small 34^{-1} cm separation in these two modes excludes the possibility of the mono-dentate adsorption of bicarbonate as this species exhibit a significantly red-shifted B_2 mode.[54] The bleach of these resonances indicates that carbonate desorbs at potentials ≤ –0.68 V (**Figure 4b**). We also observe a slight rise of a positive-going band at 1643 cm^{-1} over the same potential range, attributed to the δHOH bending mode of interfacial water[48–50] (**Figure 4b**). We observe that the integrated band intensity for carbonate (**Figure 4d**, dark blue diamonds) decreases monotonically beginning at –0.56 V, reaching a potential-invariant plateau at –0.97 V. This decline in the adsorbed carbonate band mirrors the rise and plateau in the CO_{atop} band (**Figure 4c**), suggesting that carbonate desorption is correlated with CO adsorption. From –0.76 V vs SHE to –1.05 V vs SHE, we find that the integrated band intensity for interfacial water (**Figure 4d**, light blue squares) remains unchanged within error, indicating that CO adsorption is not correlated with changes in the interfacial

water structure over this potential range. We note, however, that we do observe a correlation in the rise of the interfacial water band intensity between –0.68 V and –0.76 V vs SHE with the integrated band intensity of CO_{atop} (**Figure 4c** and **d**). Therefore, we cannot rule out that changes in the interfacial water structure do not contribute to CO adsorption in this 80 mV potential range. Together, these data indicate that CO adsorption is predominantly coincident with carbonate desorption.

Electrochemical data provide additional support for the role of carbonate desorption as the main factor gating CO adsorption on Cu. Desorption of the carbonate dianion would give rise to compensatory charge flow from the external circuit and a corresponding voltammetric feature. Indeed, CO adsorption in phosphate electrolytes is accompanied by a reversible voltammetric feature for the desorption of phosphate from the Cu surface.[43,60–64] Surface redox waves have also been shown for polycrystalline Cu electrodes cycled in CO-saturated (bi)carbonate electrolytes at pH 10.3 and have been correlated to the appearance of CO bands in FTIR spectra.[43] We reasoned that we should also be able to observe similar voltammetric features on Cu under the conditions used in this study. While the large catalytic wave observed in the slow CV scans recorded during SEIRAS measurements obscure the observation of surface electrodesorption waves, Cu foil electrodes examined at a higher scan rate under identical conditions display two broad and reversible voltammetric features at –0.71 and –0.89 V (**Figure 4a**, dotted lines). The redox waves shift by a 41±5 mV and a 44±4 mV per $\log[CO_3^{2-}]$ dec^{-1} for the first and second electrosorption peak, respectively (**Figure 4a**, inset), and display similar dependence at alternative scan rates (**Figure S13**). The observation of two reversible voltammetric features in **Figure 4a** suggests that there are two reversible CO sites. Indeed, at potential values ≤ –0.80 V, we observe the rise of a sharp shoulder in the CO_{atop} band at 2079 cm^{-1}, **Figure 4b**. This transition also coincides with an inflection point at roughly –0.80 V in the CO_{atop} integrated band intensity, **Figure 4c**, suggesting that the CO_{atop} band predominately reflects one Cu binding site at potentials more positive than –0.80 V and another site at potentials more negative than –0.80 V. While the asymmetry and the large width of the aggregate CO_{atop} peak may also suggest Fano-type coupling of CO vibrations with metal-based absorptions,[65–69] the correlation with the voltammetry waves suggest that two distinct CO binding environments are contributing to the observed peak shape. Conversely, if changes in the structure of the interfacial water were the main driver for CO adsorption, we would not observe two voltammetric features (**Figure 4a**) that: (1) shift in response to changes in CO_3^{2-} concentration in CO-saturated (bi)carbonate electrolytes; and (2) correspond with the spectral observation of two distinct CO binding environments. Taken together, the observation of two CO_3^{2-} concentration-dependent voltammetric features that coincide with two distinct binding environments for adsorbed CO further support the notion that carbonate desorption gates CO binding to the Cu surface.

The data in **Figure 4** are consistent with an electrosorptive process for CO_{atop} adsorption on Cu surfaces described by the following expression and schematically shown in **Figure 3b**,

$$Cu\text{-}CO_{atop} + CO_3^{2-}{}_{sol} \rightleftharpoons 2e^- + CO_{sol} + Cu\text{-}CO_3,$$

where CO_{aq} is the CO dissolved in the electrolyte, $Cu\text{-}CO_3$ denotes specifically-adsorbed carbonate molecules, $Cu\text{-}CO_{atop}$ denotes surface-bound CO_{atop}, $CO_3^{2-}{}_{aq}$ denotes carbonate anions in the bulk solution. This equilibrium expression highlights that reversible CO_{atop} binding to Cu surfaces is accompanied by carbonate desorption. The equilibrium potential for this reaction is given by,

$$E = E^0 + \frac{RT}{2F}\ln\left(\frac{\theta_{CO_3} a_{CO}}{\theta_{CO_{atop}} a_{CO_3^{2-}}}\right)$$

where E^0 refers to the standard state potential for the reaction, θ_{CO_3} refers to the surface coverage of carbonate, a_{CO} refers to the activity of CO, θ_{COatop} refers to the surface coverage of CO_{atop}, $a_{CO_3^{2-}}$ refers to the activity of carbonate, and the other constants take their usual meaning. This expression captures the ~30 mV/log[$c_{CO_3^{2-}}$] dependence on the electrosorptive process. Despite the large error in our measurements, our observed values of 41±5 mV and a 44±4 mV mV/log[$c_{CO_3^{2-}}$] are more in line with a two-electron electrosorptive process of carbonate than a versus a one-electron electrosorptive process of bicarbonate, which would lead to a 60 mV dec^{-1} dependence. None-the-less, we cannot rule out the possibility that bicarbonate and carbonate are simultaneously in competition with CO, giving rise to a slightly higher slope. Our conclusion is further corroborated by the spectral observable of 1543 and 1509 cm^{-1}, which correspond to carbonate and not (bi)carbonate on copper. The above equilibrium indicates that the CO surface population is governed by both the CO affinity at a given surface site and the corresponding binding energy of carbonate. Thus, the ~200 mV separation between the two surface waves reflects difference in the free energy of binding CO or CO_3^{2-} or both to the two distinct surface environments.

Comparison of Molecularity of CO Electrosorption on Au and Cu. The above studies establish the molecular basis for reversible CO binding to Au and Cu surfaces. Our studies highlight that, unlike for gas-solid interfaces, in an electrochemical environment, competitive binding of solvent and electrolyte defines the potential-dependent surface CO affinity. On Au surfaces, we show that CO_{atop} electrosorption is in competition with interfacial water and that the large dipole moment of water stabilizes the interfacial field better than bound CO at potentials positive or negative of the PZC. Thus, water adsorption drives CO desorption under the negative potentials required for CO_2RR, **Figure 3a** (yellow shaded region), explaining the wide-spread observation of selective CO production on Au surfaces.[36] In contrast, on Cu surfaces, CO_{atop} binding is driven by carbonate desorption, and the potential dependence of the latter serves to define the CO surface population during CO_2RR, **Figure 3b** (yellow shaded region). The electrochemically driven desorption of carbonate allows for the accumulation of CO on the Cu surface, priming this critical intermediate for subsequent reduction to higher order hydrocarbons and oxygenates. Together, our studies demonstrate that competing interactions with solvent and electrolyte define the equilibria that dictate CO surface population and provide a basis for explaining the divergent CO_2 reduction reactivity profiles of Au and Cu surfaces.

CONCLUSION

In this work, we utilize *in situ* infrared spectroelectrochemistry to examine the factors that control CO adsorption to Au and Cu surfaces under conditions relevant to CO_2RR catalysis. While gas phase studies establish that CO binds more strongly to Cu than Au, our studies show that the CO surface population is not governed by these intrinsic thermochemical differences alone, but is actually reflective of different CO binding equilib-

ria for Au and Cu under electrochemical conditions. On Au, reversible CO binding is driven by substitution and reorientation of adsorbed water. In contrast, CO binding to Cu requires the reductive displacement of adsorbed carbonate anions. These contrasting CO adsorption equilibria on Au and Cu leads to a large ~600 mV difference in the potential range where CO adsorption is favoured. These changes in the CO adsorption equilibria also explain divergent CO_2RR reactivity: water adsorption drives CO liberation from Au catalysts, impeding further reduction, whereas carbonate desorption drives CO accumulation on Cu, allowing for further reduction to higher order products.

Our observations provide further insight into CO_2RR electrocatalyst design. First, optimization of the CO affinity, a recognized descriptor for CO_2RR catalysis, is insufficient without considering correlated changes in the binding affinity for solvent and electrolyte species. The ideal catalyst will not only have an optimal CO binding affinity but also display a low affinity for competing solvent and/or electrolyte species in order to display CO_2RR catalysis at low overpotentials. Thus, the insights provided here introduce additional descriptors that can be used to drive computational investigations of new catalyst targets, as has been recently shown for the hydrogen evolution reaction[70]. Likewise, the experimental design of the electrolyte environment can be used to direct catalyst selectivity. By choosing strongly coordinating electrolyte ions, solvents and/or additives that compete effectively for adsorbed CO, one can turn off downstream reduction pathways. Alternatively, by pairing weakly coordinating electrolytes and solvents with appropriate catalysts such as Cu, CO species will accumulate at lower overpotentials, thereby exposing more efficient catalysis for highly reduced hydrocarbons and oxygenates. In aggregate, this study highlights, that at both a theoretical and experimental level, the directed design of efficient CO_2RR catalysts requires a revised paradigm that emphasizes the potential-dependent competitive binding of intermediates, electrolyte, and solvent in defining the free-energy profile of CO_2-to-fuels catalysis.

ASSOCIATED CONTENT

Supporting Information. Full experimental details and methods are listed in the SI. Spectra at various CO partial pressures, accompanying cyclic voltammograms, Stark tuning slopes, and control experiments without CO addition are contained in the SI. This material is available free of charge via the Internet at http://pubs.acs.org.

AUTHOR INFORMATION

Corresponding Author

* yogi@mit.edu

Present Addresses

† Department of Chemistry, University of California, Berkeley, California, United States

ACKNOWLEDGMENT

We gratefully acknowledge Thejas S. Wesley, Sahr Khan, Michael Pegis, and Daniel Nocera for insightful discussions. This research was supported by the This work is supported by the Air Force Office of Scientific Research (AFOSR) under award number FA9550-18-1-0420. A.W. acknowledges support from the Graduate Research Fellowship from the National Science Foundation. J.R. acknowledges support from a Samsung Scholarship. Y.S. acknowledges the Sloan Foundation, Research Corporation for Science Advancement (Cottrell Scholar), and the Canadian Institute for Advanced Research (CIFAR Azrieli Global Scholar).

REFERENCES

(1) Whipple, D. T.; Kenis, P. J. A. Prospects of CO_2 Utilization via Direct Heterogeneous Electrochemical Reduction. *J. Phys. Chem. Lett.* **2010**, *1* (24), 3451–3458.

(2) Olah, G. A.; Prakash, G. K. S.; Goeppert, A. Anthropogenic Chemical Carbon Cycle for a Sustainable Future. *J. Am. Chem. Soc.* **2011**, *133* (33), 12881–12898.

(3) Kortlever, R.; Peters, I.; Balemans, C.; Kas, R.; Kwon, Y.; Mul, G.; Koper, M. T. M. Palladium-Gold Catalyst for the Electrochemical Reduction of CO_2 to C_1-C_5 Hydrocarbons. *Chem. Commun.* **2016**, *52* (67), 10229–10232.

(4) Kuhl, K. P.; Hatsukade, T.; Cave, E. R.; Abram, D. N.; Kibsgaard, J.; Jaramillo, T. F. Electrocatalytic Conversion of Carbon Dioxide to Methane and Methanol on Transition Metal Surfaces. *J. Am. Chem. Soc.* **2014**, *136* (40), 14107–14113.

(5) Eilert, A.; Cavalca, F.; Roberts, F. S.; Osterwalder, J.; Liu, C.; Favaro, M.; Crumlin, E. J.; Ogasawara, H.; Friebel, D.; Pettersson, L. G. M.; et al. Subsurface Oxygen in Oxide-Derived Copper Electrocatalysts for Carbon Dioxide Reduction. *J. Phys. Chem. Lett.* **2017**, *8* (1), 285–290.

(6) Hori, Y.; Kikuchi, K.; Suzuki, S. Production of CO and CH_4 in Electrochemical Reduction of CO_2 at Metal Electrodes in Aqueous Hydrogencarbonate Solution. *Chem. Lett.* **1985**, No. 11, 1695–1698.

(7) Peterson, A. A.; Nørskov, J. K. Activity Descriptors for CO 2 Electroreduction to Methane on Transition-Metal Catalysts. *J. Phys. Chem. Lett.* **2012**, *3* (2), 251–258.

(8) Gattrell, M.; Gupta, N.; Co, A. A Review of the Aqueous Electrochemical Reduction of CO_2 to Hydrocarbons at Copper. *J. Electroanal. Chem.* **2006**, *594* (1), 1–19.

(9) Kortlever, R.; Shen, J.; Schouten, K. J. P.; Calle-Vallejo, F.; Koper, M. T. M. Catalysts and Reaction Pathways for the Electrochemical Reduction of Carbon Dioxide. *J. Phys. Chem. Lett.* **2015**, *6* (20), 4073–4082.

(10) Zhu, W.; Zhang, Y.-J.; Zhang, H.; Lv, H.; Li, Q.; Michalsky, R.; Peterson, A. A.; Sun, S. Active and Selective Conversion of CO_2 to CO on Ultrathin Au Nanowires. *J. Am. Chem. Soc.* **2014**, *136* (46), 16132–16135.

(11) Mistry, H.; Reske, R.; Zeng, Z.; Zhao, Z.-J.; Greeley, J.; Strasser, P.; Cuenya, B. R. Exceptional Size-Dependent Activity Enhancement in the Electroreduction of CO_2 over Au Nanoparticles. *J. Am. Chem. Soc.* **2014**, *136* (47), 16473–16476.

(12) Zhu, W.; Michalsky, R.; Metin, O.; Lv, H.; Guo, S.; Wright, C. J.; Sun, X.; Peterson, A. A.; Sun, S. Monodisperse Au Nanoparticles for Selective Electrocatalytic Reduction of CO_2 to CO. *J. Am. Chem. Soc.* **2013**, *135* (45), 16833–16836.

(13) Liu, M.; Pang, Y.; Zhang, B.; De Luna, P.; Voznyy, O.; Xu, J.; Zheng, X.; Dinh, C. T.; Fan, F.; Cao, C.; et al. Enhanced Electrocatalytic CO_2 reduction via Field-Induced Reagent Concentration. *Nature* **2016**, *537* (7620), 382–386.

(14) Hansen, H. A.; Varley, J. B.; Peterson, A. A.; Nørskov, J. K. Understanding Trends in the Electrocatalytic Activity of Metals and Enzymes for CO 2 Reduction to CO. *J. Phys. Chem. Lett.* **2013**, *4* (3), 388–392.

(15) Shi, C.; Hansen, H. A.; Lausche, A. C.; Nørskov, J. K. Trends in Electrochemical CO_2 Reduction Activity for Open and Close-Packed Metal Surfaces. *Phys. Chem. Chem. Phys.* **2014**, *16* (10), 4720–4727.

(16) Kim, D.; Resasco, J.; Yu, Y.; Asiri, A. M.; Yang, P. Synergistic Geometric and Electronic Effects for Electrochemical Reduction of Carbon Dioxide Using Gold-Copper Bimetallic Nanoparticles. *Nat. Commun.* **2014**, *5*, 4948.

(17) Verdaguer-Casadevall, A.; Li, C. W.; Johansson, T. P.; Scott, S. B.; Joseph, M.; Kumar, M.; Stephens, I. E. L.; Kanan, M. W.; Chorkendorff, I. Probing the Active Surface Sites for CO Reduction on Oxide- Derived Copper Electrocatalysts. *J. Am. Chem. Soc.* **2015**, *137*, 9808–9811.

(18) Asadi, M.; Kim, K.; Liu, C.; Addepalli, A. V.; Abbasi, P.; Yasaei, P.; Phillips, P.; Behranginia, A.; Cerrato, J. M.; Haasch, R.; et al. Nanostructured Transition Metal Dichalcogenide Electrocatalysts for CO_2 Reduction in Ionic Liquid. *Science (80-.).* **2016**, *353* (6298), 467–470.

(19) Nørskov, J. K.; Bligaard, T.; Logadottir, A.; Kitchin, J. R.; Chen, J. G.; Pandelov, S.; Stimming, U. Trends in the Exchange Current for Hydrogen Evolution. *J. Electrochem. Soc.* **2005**, *152*, J23.

(20) Huang, Y.; Handoko, A. D.; Hirunsit, P.; Yeo, B. S. Electrochemical Reduction of CO_2 Using Copper Single-Crystal Surfaces: Effects of CO* Coverage on the Selective Formation of Ethylene. *ACS Catal.* **2017**, *7* (3), 1749–1756.

(21) Gileadi, E. Electrosorption. In *Physical Electrochemistry, Fundamentals, Techniques and Applications*; Wiley-VCH: Weinheim, 2011; pp 175–194.

(22) Bockris, J. O.; Devanathan, M. A. V.; Muller, K. On the Structure of Charged Interfaces. *Proc. R. Soc. A Math. Phys. Eng. Sci.* **1963**, *274* (1356), 55–79.

(23) Bockris, J. O.; Reddy, A.; Gambou-Aldeco, M. E. The Electrified Interface. In *Modern Electrochemistry 2A Fundamentals of Electrodics*; Kluwer Academic/Plenum Publishers: New York, 2002; pp 933–984.

(24) Gileadi, E. The Combined Adsorption Isotherm. *Electrochim. Acta* **1987**, *32* (2), 221–229.

(25) Gileadi, E. On the Potential Dependence of Electrosorption of Neutral Organic Molecules. *J. Electroanal. Chem.* **1971**, *30* (1), 123–128.

(26) Bockris, J. O.; Jeng, K. T. In-Situ Studies of Adsorption of Organic Compounds on Platinum Electrodes. *J. Electroanal. Chem.* **1992**, *330* (1–2), 541–581.

(27) Blomgren, E.; Bockris, J. O. M.; Jesch, C. The Adsorption of Butyl, Phenyl and Naphthyl Compounds at the Interface Mercury-Aqueous Acid Solution. *J. Phys. Chem.* **1961**, *65* (11), 2000–2010.

(28) Heiland, W.; Gileadi, E.; Bockris, J. O. M. Kinetic and Thermodynamic Aspects of the Electrosorption of Benzene on Platinum Electrodes. *J. Phys. Chem.* **1966**, *70* (4), 1207–1216.

(29) Gileadi, E.; Rubin, B. T.; Bockris, J. O. M. Electrosorption of Ethylene on Platinum as a Function of Potential, Concentration, and Temperature. *J. Phys. Chem.* **1965**, *69* (10), 3335–3345.

(30) Osawa, M. Dynamic Processes in Electrochemical Reactions Studied by Surface-Enhanced Infrared Absorption Spectroscopy(SEIRAS). *Bull. Chem. Soc. Jpn.* **1997**, *70*, 2861–2880.

(31) Osawa, M. Surface Enhanced Infrared Absorption Spectroscopy. In *Handbook of Vibrational Spectroscopy*; Chalmers, J. M., Griffiths, P. R., Eds.; Wiley-VCH: Chichester, UK, 2002; pp 785–800.

(32) Osawa, M. In-Situ Surface-Enhanced Infrared Spectroscopy of the Electrode/Solution Interface. In *Diffraction and Spectroscopic Methods in Electrochemistry (Advances in Electrochemical Science and Engineering, Vol.9)*; Alkire, R. C., Kolb, D. M., Lipkowski, J., Ross, P. N., Eds.; Wiley-VCH: New York, 2006; pp 269–314.

(33) Osawa, M. Surface-Enhanced Infrared Absorption. In *Near-Field Optics and Surface Plasmon Polaritons. Topics in Applied Physics*; Kawata, S., Ed.; Springer: Berlin, 2001; Vol. 81, pp 163–187.

(34) Samjeské, G.; Komatsu, K.; Osawa, M. Dynamics of CO Oxidation on a Polycrystalline Platinum Electrode: A Time-Resolved Infrared Study. *J. Phys. Chem. C* **2009**, *113*, 10222–10228.

(35) Wuttig, A.; Liu, C.; Peng, Q.; Yaguchi, M.; Hendon, C. H.; Motobayashi, K.; Ye, S.; Osawa, M.; Surendranath, Y. Tracking a Common Surface-Bound Intermediate during CO_2 -to-Fuels Catalysis. *ACS Cent. Sci.* **2016**, *2* (8), 522–528.

(36) Wuttig, A.; Yaguchi, M.; Motobayashi, K.; Osawa, M.; Surendranath, Y. Inhibited Proton Transfer Enhances Au-Catalyzed CO_2 -to-Fuels Selectivity. *Proc. Natl. Acad. Sci.* **2016**, *113* (32), E4585–E4593.

(37) Gunathunge, C. M.; Li, X.; Li, J.; Hicks, R. P.; Ovalle, V. J.; Waegele, M. M. Spectroscopic Observation of Reversible Surface Reconstruction of Copper Electrodes under CO_2 Reduction. *J. Phys. Chem. C* **2017**, *121* (22), 12337–12344.

(38) Dunwell, M.; Lu, Q.; Heyes, J. M.; Rosen, J.; Chen, J. G.; Yan, Y.; Jiao, F.; Xu, B. The Central Role of Bicarbonate in the Electrochemical Reduction of Carbon Dioxide on Gold. *J. Am. Chem. Soc.* **2017**, *139*, 3774–3783.

(39) Heyes, J.; Dunwell, M.; Xu, B. CO_2 Reduction on Cu at Low Overpotentials with Surface-Enhanced in Situ Spectroscopy. *J. Phys. Chem. C* **2016**, *120* (31), 17334–17341.

(40) Zhu, S.; Jiang, B.; Cai, W. Bin; Shao, M. Direct Observation on Reaction Intermediates and the Role of Bicarbonate Anions in CO_2 Electrochemical Reduction Reaction on Cu Surfaces. *J. Am. Chem. Soc.* **2017**, *139* (44), 15664–15667.

(41) Hori, Y.; Murata, A. 1985; Ira; Kikuchi, K.; Suzuki, S. Electrochemical Reduction of Carbon Dioxides to Carbon Monoxide at a Gold Electrode in Aqueous Potassium Hydrogen Carbonate. *J. Chem. Soc. Chem. Commun.* **1987**, No. 10, 728–729.

(42) Hori, Y.; Murata, A.; Takahashi, R. Formation of Hydrocarbons in the Electrochemical Reduction of Carbon Dioxide at a Copper Electrode in Aqueous Solution. *J. Chem. Soc. Faraday Trans. 1 Phys. Chem. Condens. Phases* **1989**, *85* (8), 2309–2326.

(43) Hori, Y.; Koga, O.; Watanabe, Y.; Matsuo, T. FTIR Measurements of Charge Displacement Adsorption of CO on Poly- and Single Crystal (100) of Cu Electrodes. *Electrochim. Acta* **1998**, *44* (8–9), 1389–1395.

(44) Wuttig, A.; Yaguchi, M.; Motobayashi, K.; Osawa, M.; Surendranath, Y. Inhibited Proton Transfer Enhances Au-Catalyzed CO_2 -to-Fuels Selectivity. *Proc. Natl. Acad. Sci.* **2016**, *113* (32), E4585–E4593.

(45) Dunwell, M.; Yang, X.; Yan, Y.; Xu, B. Potential Routes and Mitigation Strategies for Contamination in Interfacial Specific Infrared Spectroelectrochemical Studies. *J. Phys. Chem. C* **2018**.

(46) Blizanac, B. B.; Arenz, M.; Ross, P. N.; Marković, N. M. Surface Electrochemistry of CO on Reconstructed Gold Single Crystal Surfaces Studied by Infrared Reflection Absorption Spectroscopy and Rotating Disk Electrode. *J. Am. Chem. Soc.* **2004**, *126*, 10130–10141.

(47) Bode, D. D.; Andersen, T. N.; Eyring, H. Anion and PH Effects on the Potentials of Zero Charge of Gold and Silver Electrodes. *J. Phys. Chem.* **1967**, *71* (4), 792–797.

(48) Ataka, K.; Yotsuyanagi, T.; Osawa, M. Potential-Dependent Reorientation of Water Molecules at an Electrode/Electrolyte Interface Studied by Surface-Enhanced Infrared Absorption Spectroscopy. *J. Phys. Chem.* **1996**, *100*, 10664–10672.

(49) Ataka, K.; Osawa, M. In Situ Infrared Study of Water−Sulfate Coadsorption on Gold(111) in Sulfuric Acid Solutions. *Langmuir* **1998**, *14* (4), 951–959.

(50) Osawa, M.; Tsushima, M.; Mogami, H.; Samjeské, G.; Yamakata, A. Structure of Water at the Electrified Platinum−Water Interface: A Study by Surface-Enhanced Infrared Absorption Spectroscopy. *J. Phys. Chem. C* **2008**, *112*, 4248–4256.

(51) Berná, A.; Rodes, A.; Feliu, J. M.; Illas, F.; Gil, A.; Clotet, A.; Ricart, J. M. Structural and Spectroelectrochemical Study of Carbonate and Bicarbonate Adsorbed on Pt(111) and Pd/Pt(111) Electrodes. *J. Phys. Chem. B* **2004**, *108*, 17928–17939.

(52) Arihara, K.; Kitamura, F.; Ohsaka, T.; Tokuda, K. Characterization of the Adsorption State of Carbonate Ions at the Au(111) Electrode Surface Using in Situ IRAS. *J. Electroanal. Chem.* **2001**, *510* (1–2), 128–135.

(53) Krishnamurty, K. V.; Harris, G. M.; Sastri, V. S. The Chemistry of the Metal Carbonato Complexes. *Chem. Rev.* **1970**, *70* (2), 171–197.

(54) Fujita, J.; Martell, A. E.; Nakamoto, K. Infrared Spectra of Metal Chelate Compounds. VIII. Infrared Spectra of Co (III) Carbonato Complexes. *J. Chem. Phys.* **1962**, *36* (2), 339–345.

(55) Wang, H.-F.; Yan, Y.-G.; Huo, S.-J.; Cai, W.-B.; Xu, Q.-J.; Osawa, M. Seeded Growth Fabrication of Cu-on-Si Electrodes for in Situ ATR-SEIRAS Applications. *Electrochim. Acta* **2007**, *52*, 5950–5957.

(56) Pritchard, J.; Catterick, T.; Gupta, R. K. Infrared Spectroscopy of Chemisorbed Carbon Monoxide on Copper. *Surf. Sci.* **1975**, *53* (1), 1–20.

(57) Salimon, J.; Hernández-Romero, R. M.; Kalaji, M. The Dynamics of the Conversion of Linear to Bridge Bonded CO on Cu. *J. Electroanal. Chem.* **2002**, *538–539*, 99–108.

(58) Gunathunge, C. M.; Ovalle, V. J.; Li, Y.; Janik, M. J.; Waegele, M. M. Existence of an Electrochemically Inert CO Population on

Cu Electrodes in Alkaline PH. *ACS Catal.* **2018**, *8* (8), 7507–7516.

(59) Greenaway, A. M.; Dasgupta, T. P.; Koshy, K. C.; Sadler, G. G. A Correlation between Infrared Stretching Mode Absorptions and Structural Angular Distortions for the Carbonato Ligand in a Wide Variety of Complexes. *Spectrochim. Acta Part A Mol. Spectrosc.* **1986**, *42* (9), 949–954.

(60) Hori, Y.; Murata, A.; Tsukamoto, T.; Wakebe, H.; Koga, O.; Yamazaki, H. Adsorption of Carbon Monoxide at a Copper Electrode Accompanied by Electron Transfer Observed by Voltammetry and IR Spectroscopy. *Electrochim. Acta* **1994**, *39*, 2495–2500.

(61) Hori, Y.; Koga, O.; Yamazaki, H.; Matsuo, T. Infrared Spectroscopy of Adsorbed CO and Intermediate Species in Electrochemical Reduction of CO_2 to Hydrocarbons on a Cu Electrode. *Electrochim. Acta* **1995**, *40* (16), 2617–2622.

(62) Koga, O.; Watanabe, Y.; Tanizaki, M.; Hori, Y. Specific Adsorption of Anions on a Copper (100) Single Crystal Electrode Studied by Charge Displacement by CO Adsorption and Infrared Spectroscopy. *Electrochim. Acta* **2001**, *46* (20–21), 3083–3090.

(63) Hori, Y.; Wakebe, H.; Tsukamoto, T.; Koga, O. Adsorption of CO Accompanied with Simultaneous Charge Transfer on Copper Single Crystal Electrodes Related with Electrochemical Reduction of CO_2 to Hydrocarbons. *Surf. Sci.* **1995**, *335* (C), 258–263.

(64) Koga, O.; Matsuo, T.; Hoshi, N.; Hori, Y. Charge Displacement Adsorption of Carbon Monoxide on [110] Zone Copper Single Crystal Electrodes in Relation with PZC. *Electrochim. Acta* **1998**, *44* (6–7), 903–907.

(65) Wu, C.-X.; Lin, H.; Chen, Y.-J.; Li, W.-X.; Sun, S.-G. Abnormal IR Effects of Pt Nanostructured Surfaces upon CO Chemisorption Due to Interaction and Electron-Hole Damping. *J. Chem. Phys.* **2004**, *121*, 1553–1556.

(66) Su, Z.-F.; Sun, S.-G.; Wu, C.-X.; Cai, Z.-P. Study of Anomalous Infrared Properties of Nanomaterials through Effective Medium Theory. *J. Chem. Phys.* **2008**, *129*, 044707-1–6.

(67) Krauth, O.; Fahsold, G.; Magg, N.; Pucci, A. Anomalous Infrared Transmission of Adsorbates on Ultrathin Metal Films: Fano Effect near the Percolation Threshold. *J. Chem. Phys.* **2000**, *113*, 6330–6333.

(68) Wang, H. C.; Sun, S. G.; Yan, J. W.; Yang, H. Z.; Zhou, Z. Y. In Situ STM Studies of Electrochemical Growth of Nanostructured Ni Films and Their Anomalous IR Properties. *J. Phys. Chem. B* **2005**, *109*, 4309–4316.

(69) Priebe, A.; Sinther, M.; Fahsold, G.; Pucci, A. The Correlation between Film Thickness and Adsorbate Line Shape in Surface Enhanced Infrared Absorption. *J. Chem. Phys.* **2003**, *119*, 4887–4890.

(70) Cheng, T.; Wang, L.; Merinov, B. V.; Goddard, W. A. Explanation of Dramatic PH-Dependence of Hydrogen Binding on Noble Metal Electrode: Greatly Weakened Water Adsorption at High PH. *J. Am. Chem. Soc.* **2018**, *140* (25), 7787–7790.